Magnetic interference patterns in 0-π superconductor/insulator/ferromagnet/superconductor Josephson junctions: Effects of asymmetry between 0 and π regions

M. Kemmler,[1,*] M. Weides,[2,†] M. Weiler,[3] M. Opel,[3] S. T. B. Goennenwein,[3] A. S. Vasenko,[4] A. A. Golubov,[5] H. Kohlstedt,[6] D. Koelle,[1] R. Kleiner,[1] and E. Goldobin[1]

[1]*Physikalisches Institut–Experimentalphysik II and Center for Collective Quantum Phenomena, Universität Tübingen, Auf der Morgenstelle 14, D-72076 Tübingen, Germany*

[2]*Institute of Solid State Research and JARA–Fundamentals of Future Information Technology, Research Centre Jülich, D-52425 Jülich, Germany*

[3]*Walther-Meissner-Institut, Bayerische Akademie der Wissenschaften, D-85748 Garching, Germany*

[4]*LPMMC, Université Joseph Fourier and CNRS, 25 Avenue des Martyrs, BP 166, 38042 Grenoble, France*

[5]*Faculty of Science and Technology and MESA+ Institute for Nanotechnology, University of Twente, 7500 AE Enschede, The Netherlands*

[6]*Nanoelektronik, Technische Fakultät, Christian-Albrechts-Universität zu Kiel, D-24143 Kiel, Germany*

(Received 27 October 2009; revised manuscript received 4 February 2010; published 26 February 2010)

We present a detailed analysis of the dependence of the critical current I_c on an in-plane magnetic field B of 0, π, and 0-π superconductor-insulator-ferromagnet-superconductor Josephson junctions. $I_c(B)$ of the 0 and the π junction closely follows a Fraunhofer pattern, indicating a homogeneous critical current density $j_c(x)$. The maximum of $I_c(B)$ is slightly shifted along the field axis, pointing to a small remanent in-plane magnetization of the F-layer along the field axis. $I_c(B)$ of the 0-π junction exhibits the characteristic central minimum. I_c, however, has a finite value here, due to an asymmetry of j_c in the 0 and the π part. In addition, this $I_c(B)$ exhibits asymmetric maxima and bumped minima. To explain these features in detail, flux penetration being different in the 0 part and the π part needs to be taken into account. We discuss this asymmetry in relation to the magnetic properties of the F-layer and the fabrication technique used to produce the 0-π junctions.

DOI: 10.1103/PhysRevB.81.054522 PACS number(s): 74.50.+r, 74.78.Fk, 85.25.Cp

I. INTRODUCTION

While predicted more than 30 years ago,[1,2] due to the severe technological requirements, the experimental study of π Josephson junctions became an intense field of research only recently. Superconductor-ferromagnet-superconductor (SFS) Josephson junctions were successfully fabricated and studied.[3–6] SFS junctions, however, typically exhibit only very small (metallic) resistances R, making this type of junctions less suitable for the study of dynamic junction properties as well as for applications, where active Josephson junctions are required. To overcome this problem, an additional insulating (I) layer can be used to increase R, although at the expense of a highly reduced critical current density j_c.[7–10]

In a SFS or SIFS junction, the proximity effect in the ferromagnetic layer leads to a damped oscillation of the superconducting order parameter in the F-layer. Thus, depending on the thickness d_F of the F-layer, the sign of the order parameters in the superconducting electrodes may be the same or not. While in the first case, a conventional Josephson junction (a "0 junction") with $I_s=I_c \sin(\mu)$ is realized, in the latter case a "π junction" is formed where the Josephson current I_s obeys the relation $I_s=I_c \sin(\mu+\pi)=-I_c \sin(\mu)$. Here $I_c \geq 0$ is the junction critical current and μ is the phase difference of the order parameters in the two electrodes.

The combination of a 0 and a π part within a single Josephson junction leads to a "0-π" Josephson junction. Depending on several parameters of the 0 and the π part, a spontaneous fractional vortex may appear at the 0-π boundary.[11] In case of long junctions with length $L \gg \lambda_J$, the vortex contains a flux equal to a half of a flux quantum $\Phi_0 \approx 2.07 \times 10^{-15}$ Tm^2. Here $\lambda_J \approx \sqrt{\Phi_0/(4\pi\mu_0 j_c \lambda_L)}$ is the Josephson length; μ_0 is the magnetic permeability of the vacuum; and λ_L is the London penetration depth of both electrodes.

Up to now, three different types of 0-π Josephson junctions or π superconducting quantum interference devices (SQUIDs) have been demonstrated experimentally. One approach makes use of the $d_{x^2-y^2}$-wave order-parameter symmetry in cuprate superconductors.[12–17] Another approach is to use standard Nb/Al-Al$_2$O$_3$/Nb Josephson junctions equipped with current injectors[18,19] which allow to create any phase shift. 0-π Josephson junctions were also produced by SFS technology.[20–22] The first intentionally made 0-π SIFS junction including reference 0 and π Josephson junctions fabricated in the same run were recently realized.[23] Some static and dynamic properties of this type of 0-π junction were studied experimentally.[23–25] Relevant theoretical work on SIFS junctions can be found in Refs. 26 and 27.

The aim of the present paper is to provide a careful analysis of the magnetic field dependence of the junction critical current $I_c(B)$ in order to characterize these novel type of junctions as accurately as possible. In all $I_c(B)$ measurements, the magnetic field was applied in the plane of the junction. The (short) junction we discuss has a length $L \approx \lambda_J$. As we will see, the measured $I_c(B)$ can be reproduced very well when, apart from asymmetries of the critical current densities in the 0 and the π parts, asymmetric flux penetration into the 0 and the π parts is taken into account.

The paper is organized as follows: in Sec. II, the SIFS junctions are characterized in terms of geometry, and the properties of the F-layer are further characterized by measuring the magnetization of a bare Ni$_{0.6}$Cu$_{0.4}$ thin films with thickness comparable to the F-layer used for the junctions. In

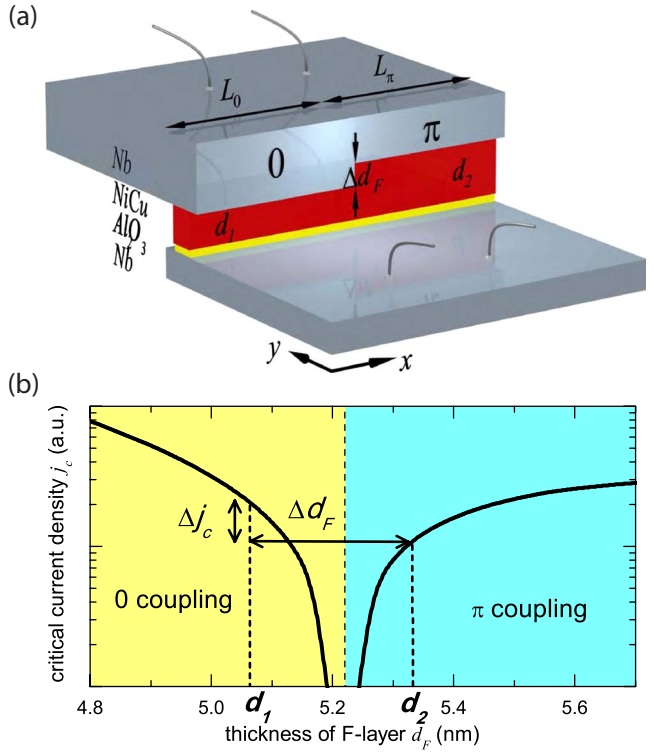

FIG. 1. (Color online) (a) Sketch of a 0-π SIFS Josephson junction with steplike F-layer to create a 0-coupled part (F-layer thickness d_1) and a π part (d_2). L_0, L_π denote the length in each part. (b) Schematic $j_c(d_F)$ dependence for SIFS Josephson junctions. For the ferromagnetic thicknesses d_1 and $d_2 = d_1 + \Delta d_F$, the critical current densities $j_c(d_1)$ and $j_c(d_2)$ have similar absolute values ($j_c(d_1) = j_c(d_2) + \Delta j_c$).

the central Sec. III, the magnetic field dependence of the critical current of the SIFS junctions is discussed. Section IV contains the conclusion.

II. SAMPLE CHARACTERIZATION

Figure 1(a) shows a sketch of the 0-π junction used in the experiment. The superconducting bottom and top layers consist of Nb with the thicknesses $t_1 = 120$ nm and $t_2 = 400$ nm, respectively. Like in standard Nb tunnel junctions, an Al_2O_3 layer was used as tunnel barrier. Its thickness of $d_I' \approx 0.9$ nm was determined from an analysis of Fiske steps in the current-voltage (IV) characteristics of various junctions. For the ferromagnetic layer, we use the diluted ferromagnet $Ni_{0.6}Cu_{0.4}$. To form a 0-π junction, the junction is divided into two parts differing by the thickness of the F-layer. While in one half of the junction, the thickness d_1 is chosen such that 0 coupling is realized, in the other half, the F-layer thickness d_2 is used to realize π coupling. In order to have approximately symmetric junctions, d_1 and d_2 should be such that the critical current densities of the two halves are about the same and as large as possible, see Fig. 1(b).

Details of the fabrication technique can be found in Refs. 24 and 28. The main feature is a gradient in the ferromagnetic $Ni_{0.6}Cu_{0.4}$ layer along the y direction of the 4 in. wafer, in order to allow for a variety of 0 and π coupled junctions

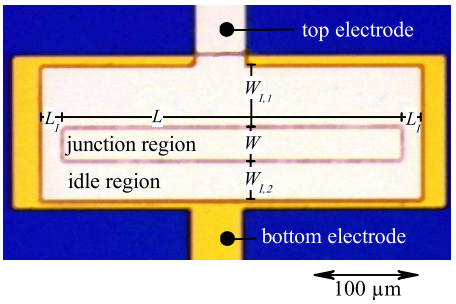

FIG. 2. (Color online) Optical image (top view) of a 330 $\times 30$ μm^2 window junction with junction and idle regions.

differing in their critical current densities. In addition, by optical lithography and controlled etching, parts of the F-layer are thinned by $\Delta d_F \approx 3$ Å, such that 0 coupling is achieved in these parts. Thus the chip contains unetched parts with F-layer thickness $d_F(y)$, as well as uniformly etched parts with F-layer thickness $d_F(y) - \Delta d_F$. Thus, at a fixed y position, we have two different ferromagnetic thicknesses allowing for patterning a set of three junctions: (1) a 0 junction with F-layer thickness d_1 and critical current density $j_c^0 \equiv j_c(d_1)$. (2) A π junction with F-layer thickness d_2 and critical current density $j_c^\pi \equiv j_c(d_2)$. (3) A stepped 0-π junction with thicknesses d_1 and d_2, and critical densities j_c^0 and j_c^π in the 0 and the π halves.

For the values $d_1 = 5.05$ nm and $d_2 = 5.33$ nm, we obtained $j_c^0 \approx 2.1$ A/cm^2 and $j_c^\pi \approx 1.7$ A/cm^2 at $T = 4.2$ K, as estimated from 0 and π reference junctions. The temperature dependence of the critical current density $j_c(T)$ of SFS and SIFS junctions depends on the ratio of d_F to the (temperature dependent) decay and oscillation lengths of the superconducting wave function in the F-layer. Thus, $j_c(T)$ strongly depends on d_F and on the slope $\partial j_c / \partial d_F$ [cf. Fig. 1(b)]. With decreasing temperature, one can obtain increasing, decreasing, or nearly constant critical current densities (see, e.g., Refs. 8 and 29). For the thicknesses d_1 and d_2 of our junctions, and for temperatures between 2.65 and 4.2 K, we find an almost constant j_c^0 whereas j_c^π increases with decreasing temperature. Due to that we get almost equal critical current densities $j_c^0 \approx j_c^\pi \approx 2.2$ A/cm^2 at $T = 2.65$ K.

All junctions had the same geometrical dimensions 330 $\times 30$ μm^2, see Fig. 2. The superconducting electrodes extend well beyond the junction area, leading to an idle region around the junction affecting the Josephson length λ_J. Ignoring this correction, using $j_c^0 = j_c^\pi = 2.2$ A/cm^2, as measured at $T = 2.65$ K, one finds $\lambda_J \approx 260$ μm, i.e., $L \approx 1.2\lambda_J$ as in Ref. 23. The idle region of width $W_{I,1} + W_{I,2}$ in y direction modifies the inductance of the electrodes and leads to an effective Josephson length,[30]

$$\lambda_{J,\mathrm{eff}} = \lambda_J \sqrt{1 + \frac{W_{I,1} + W_{I,2}}{W} \frac{d_J'}{d_I'}}$$

with the junction width W, and the inductances (per square) of the superconducting films forming the junction electrodes $\mu_0 d_J'$ and the idle regions $\mu_0 d_I'$. For our junction, we get $\lambda_{J,\mathrm{eff}} = 1.7\lambda_J$ with $W = 30$ μm, $W_{I,1} + W_{I,2} = 100$ μm, d_J'

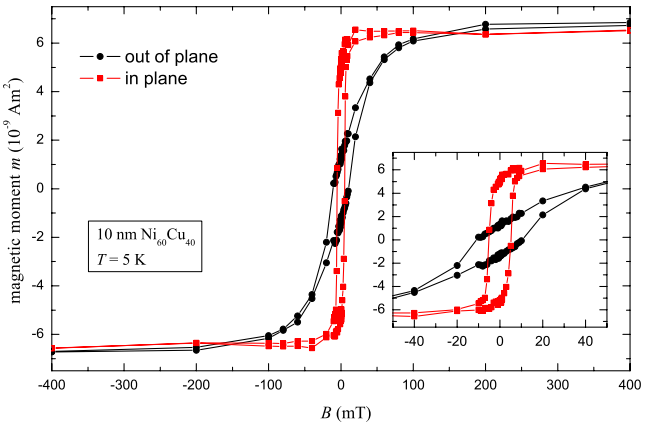

FIG. 3. (Color online) Magnetization curves of a $Ni_{0.6}Cu_{0.4}$ thin film with 10 nm thickness at $T=5$ K probed by SQUID magnetometry. The magnetic field was applied either in-plane (squares) and out-of-plane (circles). The inset shows a magnification at small magnetic fields.

$=194$ nm, and $d_I'=350$ nm. Therefore the normalized junction length at $T=2.65$ K is $l=L/\lambda_{J,\mathrm{eff}}\approx 0.76$ and we clearly are in the short junction limit.

Magnetic properties of the F-layer

In order to investigate the magnetic properties of the $Ni_{0.6}Cu_{0.4}$ alloy used for the F-layer, we performed measurements of the magnetization via SQUID magnetometry. The sample was a 10 nm thin $Ni_{0.6}Cu_{0.4}$ film deposited directly on a SiO_2 substrate. The Curie temperature $T_{\mathrm{Curie}}\approx 200$ K was determined by measuring the remanent magnetization in zero applied magnetic field during warming up after field cooling the sample to $T=120$ K with $B=100$ mT. The obtained magnetization curves (after diamagnetic correction) at $T=5$ K are shown in Fig. 3 for the magnetic field applied in-plane or out-of plane. The magnetic moments for the out-of-plane and in-plane component saturate at almost equal $m\approx 6.5\times 10^{-9}$ Am^2 corresponding to a saturation magnetization $M=130$ kA/m. Using the density $\rho=8.92$ g/cm^3 (bulk value) of the F-layer and the molar weight 60.6 g, we can estimate the atomic saturation moment $m_{\mathrm{at}}=0.16\mu_B$, in good agreement with $m_{\mathrm{at}}=0.15\mu_B$ found in literature.[31]

The hysteresis of the magnetization curves is visible in detail in the inset of Fig. 3. Remanence can be seen for the in-plane as well as the out-of-plane curves. The inversion of the magnetizations is smooth, indicating a multiple domain state. The magnetic field necessary to fully magnetize the magnetic film in-plane is in the order of 10 mT whereas the out-of-plane magnetization saturates above about 100 mT. Therefore, we expect the in-plane magnetization to be energetically favorable.

Both saturation fields are orders of magnitude larger than the in-plane fields typically used for SIFS critical current versus magnetic field measurements. In the following, we estimate an upper limit by how much the $I_c(B)$ pattern (of a 0 junction or a π junction) would shift along the field axis for an in-plane, fully saturated ferromagnetic layer. Our measured saturation magnetization $M=130$ kA/m yields a magnetic induction $\mu_0 M=0.163$ T. A cross section of length L and a thickness d_F encloses an intrinsic magnetic flux $\Phi_M=d_F L\mu_0 M$. For $L=330$ μm and $d_F=5$ nm, the magnetic flux is $\Phi_M=129\times\Phi_0$. Thus, the $I_c(B)$ pattern would be shifted along the field axis by about 129 periods while in experiment typically shifts of much less than one period are observed. Further, nearly all our SIFS junctions had mirror-symmetrical $I_c(B)$ patterns for $|B|<1$ mT, again strongly indicating that the F-layer is in a multiple domain state with a very small in-plane net magnetic flux.[32] The out-of-plane net magnetic flux has to be small too. As we will see in the next section, for the 0 and the π junctions, highly symmetric $I_c(B)$ patterns can be measured. If the out-of-plane magnetic flux were very large, one would expect a large number of Abrikosov vortices penetrating the superconducting layers, making the $I_c(B)$ of SIFS junctions with a planar F-layer strongly asymmetric.

The ferromagnetic properties of a comparable ferromagnetic compound, $Cu_{0.47}Ni_{0.53}$, were investigated recently via anomalous Hall voltage measurements and Bitter decoration techniques of the magnetic domain structures,[33] indicating a magnetic anisotropy and a magnetic structure with domains of about 100 nm in size. Both Hall and Bitter decoration measurements are only sensitive to out-of-plane components of the magnetic fields, and the growth conditions of the CuNi sample in Ref. 33 may influence its magnetic properties. Nevertheless it supports our experimental findings of a very small in-plane magnetization for zero-field-cooled samples and a multiple domain state in the F-layer of our SIFS devices.

III. CRITICAL CURRENT VS MAGNETIC FIELD

In order to measure the magnetic field dependence of the critical currents of our junctions, the samples were mounted in a glass-fiber Helium cryostat surrounded by a triple mu-metal shield. To minimize external noise, the whole setup was placed in a high-frequency screening room, the current leads were low-pass filtered, and all electronics within the screening room was powered by batteries. The sample was initially cooled from room temperature down to 4.2 K with the sample mounted inside the magnetic shield. To remove magnetic flux sometimes trapped in the superconducting electrodes, the sample was thermally cycled to above the superconducting transition temperature T_c. To determine I_c, we used a voltage criterion of $V_{\mathrm{cr}}=0.5$ μV. The IV characteristics and $I_c(B)$ were measured for all three junctions at various temperatures $T=4.2\ldots 2.65$ K. The magnetic field B was applied along the y direction see Fig. 1(a).

Figure 4 shows measurements of $I_c(B)$ at (a) $T\approx 2.65$ K and (b) $T=4.2$ K. Together with the experimental data, we plot theoretical curves using the analytic expressions valid for short junctions having homogenous critical current density.

For 0 and π junctions, one has the Fraunhofer pattern,

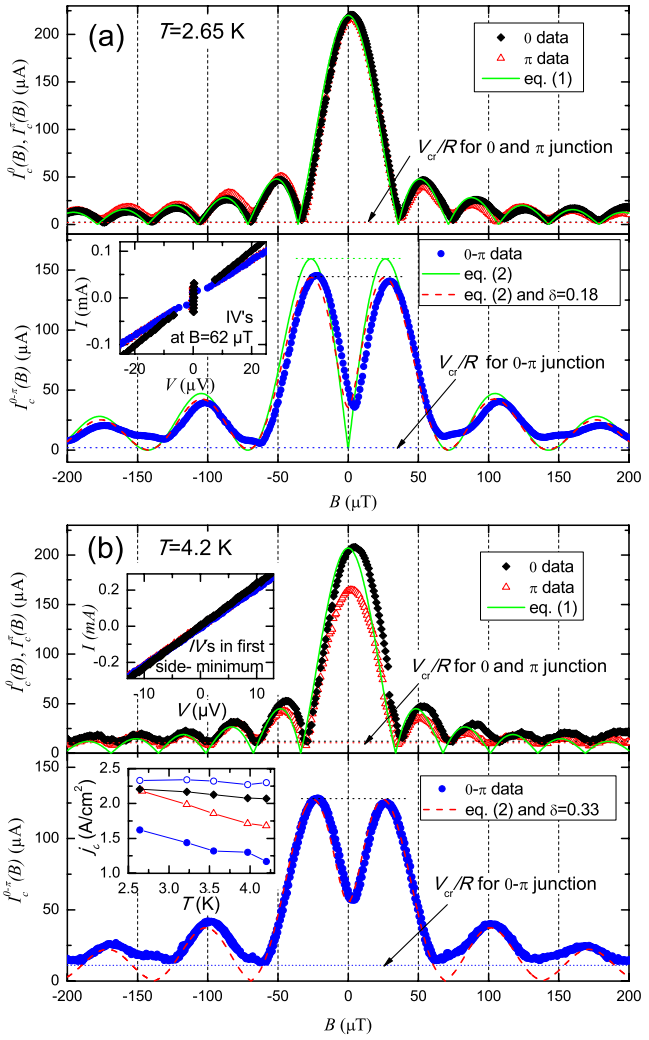

FIG. 4. (Color online) $I_c(B)$ measurements and theoretical curves (short junction model) for 0, π, and 0-π Josephson junctions at (a) $T \approx 2.65$ K and (b) $T \approx 4.2$ K. In the top graphs of (a) and (b), data for 0 and π junctions are shown by solid symbols; the Fraunhofer curves Eq. (1) are shown by the solid lines. In the lower graphs, data for the 0-π junction are shown by symbols; the solid line corresponds to Eq. (2). For the theoretical curve shown by the dashed lines, an asymmetry in the critical current densities $\delta \equiv (j_c^0 - j_c^\pi)/(j_c^0 + j_c^\pi) = 0.18$ in (a) and 0.33 in (b) has been assumed. The horizontal dotted lines show the value of $I_{c,\min}$. The inset in (a) and the upper inset in (b) show *IV* curves for all three Josephson junctions, using the same symbols as for the $I_c(B)$ patterns. The lower inset in (b) shows the measured $j_c^0(T)$ (diamonds) and $j_c^\pi(T)$ (triangles) of the reference junctions together with the $j_c^{0,\pi}(T)$ dependencies (open and filled circles) of the 0-π Josephson junction extracted from $I_c^{0\text{-}\pi}(B)$.

$$I_c^{0,\pi}(B) = I_c^{0,\pi}(0) \left| \frac{\sin\left(\frac{\pi\Phi}{\Phi_0}\right)}{\frac{\pi\Phi}{\Phi_0}} \right|, \tag{1}$$

where $\Phi/\Phi_0 = BL\Lambda/\Phi_0$ is the number of the applied flux quanta through the normalized junction area $L\Lambda$, with $\Lambda = d_I + d_F + \lambda_L \tanh(t_1/2\lambda_L) + \lambda_L \tanh(t_2/2\lambda_L)$.

For a symmetric, short 0-π junction the analytical expression is given by[14,34]

$$I_c^{0\text{-}\pi}(B) = I_c^0 \frac{\sin^2\left(\frac{\pi}{2}\frac{\Phi}{\Phi_0}\right)}{\left|\frac{\pi}{2}\frac{\Phi}{\Phi_0}\right|}. \tag{2}$$

At $T = 2.65$ K, the reference junctions have basically the same maximum critical current of $I_c^0 \approx 220$ μA and $I_c^\pi \approx 217$ μA and are fitted very well by the standard Fraunhofer curve given by Eq. (1). Note that the maximum is shifted along the B axis by a few percent of one flux quantum. For reference, we also show by a dotted horizontal line the I_c-detection limit $I_{c,\min} = V_{\rm cr}/R$ set by the finite-voltage criterion. Here R denotes the (subgap) junction resistance at small voltage. R was estimated from the corresponding *IV* curves shown in the insets of Fig. 4. For the measurements at $T = 2.65$ K, this line is marginally shifted from zero.

Looking at $I_c^{0\text{-}\pi}(B)$ of the stepped 0-π junction at $T = 2.65$ K [see bottom graph of Fig. 4(a)], we see that the agreement between the analytical expression (2) and the measurement is worse than for the reference junctions. For example, the central minimum of $I_c^{0\text{-}\pi}(B)$ is reproduced qualitatively, however, apart from a slight shift to positive magnetic field values, it does not reach zero critical current and is U shaped in contrast to the V-shaped central minimum predicted by Eq. (2). Further, the side maxima in $I_c^{0\text{-}\pi}(B)$ at the magnetic field $\pm B_m = 2\Phi_0/L\Lambda$ are below the theoretical value of $0.72 I_c^0$. Additionally, we found a small asymmetry of the maxima of 4%, i.e., $I_c^{0\text{-}\pi}(-B_m)/I_c^0 \approx 0.66$ and $I_c^{0\text{-}\pi}(+B_m)/I_c^0 \approx 0.64$. Finally, the first side minima of $I_c^{0\text{-}\pi}(B)$ were reached at the same magnetic field ($\Phi/\Phi_0 = \pm 2$) as the second minima of the $I_c(B)$ of the reference junctions but exhibit bumps and do not reach zero level defined by the $I_{c,\min}$ line.

All discrepancies to the calculated pattern, especially the nonvanishing minima, are not due to our measurement technique. All characteristic features are well above our I_c detection limit, drawn by the dotted line in the bottom graph of Fig. 4(a). The U-shaped central minimum $I_c^{0\text{-}\pi}(0)$ could be due to fluctuations in the applied magnetic field. However, careful measurements using superconducting magnetic field coils in persistent mode to exclude any magnetic field noise showed no further decrease of the I_c-minimum. An improved fit can be achieved by assuming that the critical current densities of the two halves of the 0-π junction are not identical, i.e., are different from the respective j_c^0 and j_c^π of the reference junctions (e.g., caused by some gradient of the ferromagnetic thickness along x direction; the distance between reference and stepped junctions on the chip is about 2 mm). The dashed line in the bottom graph of Fig. 4(a) shows the result of a corresponding calculation (the procedure is discussed further below) using $\delta \equiv (j_c^0 - j_c^\pi)/(j_c^0 + j_c^\pi) = 0.18$. While the critical current value of the central minimum is reproduced reasonably well, the other discrepancies remain.

Figure 4(b) shows data for $T = 4.2$ K. The critical currents of the 0 and the π reference junction differ by $\approx 22\%$ but still are reasonably well described by the Fraunhofer pattern Eq.

(2). The main discrepancy between fit and measurements can be found in the minima of $I_c(B)$. The experimental minima do not reach zero current, which at this temperature is due to the finite voltage criterion, cf. horizontal dotted lines. The lower graph in Fig. 4(b) shows the corresponding $I_c(B)$ measurement for the 0-π junction together with a theoretical curve, using δ=0.33. Although the overall agreement between the two curves is reasonable, again the shape of the minima is not reproduced well.

To further discuss the observed discrepancies, we either have to assume that j_c^0 and j_c^π are nonuniform over the junction length, which would be contradictory to the observations at the reference junctions or we should consider effects caused by a possible remanent magnetization of the F-layer, which can be different in the 0 and the π part, plus the possibility that the magnetic flux generated by the applied field may be enhanced by the magnetic moment of the F-layer. Also, the effective junction thickness Λ may be different in the 0 and the π parts, causing additional asymmetries. To account for these effects, the local phases in the two parts may be written as

$$\mu^0(x) = \phi_0 + (\varphi_B^0 + \varphi_M^0)x/L_0, \tag{3}$$

$$\mu^\pi(x) = \phi_0 + (\varphi_B^\pi + \varphi_M^\pi)x/L_\pi. \tag{4}$$

Here, ϕ_0 is an initial phase to be fixed when calculating the total critical current. $\varphi_M^{0,\pi}$ are the fluxes, normalized to $\Phi_0/2\pi$, that are generated by the (one dimensional) y component of the in-plane remanent magnetizations in the 0 and the π parts, respectively. $\varphi_B^{0,\pi}$ are the normalized fluxes through the junction generated by the applied magnetic field. In the following, we parameterize $\varphi_M^{0,\pi}$ as $\varphi_M^{0,\pi}=\bar{\varphi}_M(1\pm\delta_M)$ and $\varphi_B^{0,\pi}$ as $\varphi_B^{0,\pi}=\bar{\varphi}_B(1\pm\delta_B)$, respectively. We further set $L_0=L_\pi=L/2$ which is the case for the sample discussed here.

To obtain the junction critical current $I_c^{0\text{-}\pi}$ as a function of the applied magnetic field, we first calculate the currents I_0 and I_π in the 0 and the π parts via

$$I_0 = \int_{-L_0}^{0} j_c^0 \sin[\mu^0(x)]dx,$$

$$I_\pi = \int_{0}^{L_\pi} j_c^\pi \sin[\mu^\pi(x) + \pi]dx,$$

and maximize I_0+I_π with respect to ϕ_0 for each value of the applied magnetic field.

We first address the effect of the parameters δ, $\bar{\varphi}_M$, δ_M, and δ_B on the $I_c^{0\text{-}\pi}(\bar{\varphi}_B)$ patterns, cf. Figs. 5(a)–5(d).

If only a j_c asymmetry is considered, as shown in Fig. 5(a), using definitions $j_c^0=j_c(1+\delta)$, $j_c^\pi=j_c(1-\delta)$, and $j_c=0.5(j_c^0+j_c^\pi)$, one finds that with increasing asymmetry δ, the central minimum increases (for δ=1, one reaches the extremum of a nonstepped junction with length L_0 while the π part becomes "non-Josephson" with $j_c^\pi=0$). However in all cases, the first side maxima remain symmetric and the side minima reach zero current.

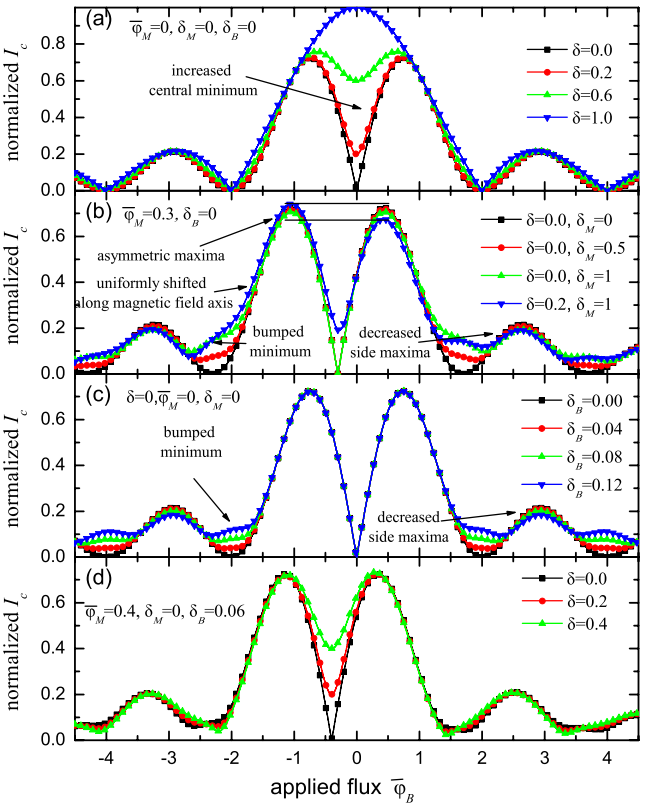

FIG. 5. (Color online) Calculated magnetic diffraction pattern $I_c^{0\text{-}\pi}(\bar{\varphi}_B)$ for a short 0-π junction with asymmetries in the critical current densities and in the magnetizations of the 0 and the π part: (a) effect of the asymmetry parameter of the critical current density δ; (b) resulting pattern with additional remanent magnetizations (average value $\bar{\varphi}_M$ and asymmetry δ_M); (c) effect of the asymmetry parameter δ_B caused by the applied flux; (d) effect of δ for nonzero values of $\bar{\varphi}_M$=0.4 and δ_B=0.06.

Next we would like to take into account the effect of the flux generated by remanent magnetizations. If we consider only a nonzero magnetization, i.e., $\bar{\varphi}_M \neq 0$, with all other parameters being zero, the $I_c(\bar{\varphi}_B)$ curve gets shifted along the field axis since the total flux in the junction is just the sum of applied field and magnetization. This can be seen in Fig. 5(b) (squares). By adding an asymmetry δ_M, the side minima get bumped and at the same time the maxima decrease [cf. Fig. 5(b) circles]. However the $I_c(\bar{\varphi}_B)$ curve is still symmetric with respect to the central minimum. This changes by adding an additional asymmetry $\delta \neq 0$ in the critical current densities. Now the two main maxima get asymmetric and the side minima get bumped (down triangles).

Now we want to consider the effect of asymmetric flux in the 0 and the π halves, i.e., we look at $\delta_B \neq 0$. In Fig. 5(c), we show the results obtained by increasing δ_B with the other parameters kept at zero. The increase in δ_B leads to bumped minima and decreased side maxima. The resulting $I_c(\bar{\varphi}_B)$ curves looks similar to the ones shown in Fig. 5(b) with asymmetries in the magnetization δ_M. The comparison reveals that the δ_B parameter acts much stronger than δ_M. The $I_c(\bar{\varphi}_B)$ curve is still symmetric with respect to the central minimum.

In Fig. 5(d), we add a remanent magnetization without asymmetry, i.e., $\bar{\varphi}_M \neq 0$ and δ_M=0, and allow asymmetric

critical currents $\delta \neq 0$. As one can see the maxima remain symmetric whereas the minima get slightly asymmetric.

We further note that the calculated $I_c(B)$ patterns are identical if we simultaneously change the sign of δ, δ_M, and δ_B. Thus the $I_c(B)$ pattern of the 0-π junction only does not allow to identify which parameters belong to the 0 and the π part. However the additional information on the (temperature dependent) critical current densities of the reference junctions [cf. Fig. 4(b) lower inset] may allow a clear identification of 0 and π.

Using the above findings on the parameters δ, $\bar{\varphi}_M$, δ_M, and δ_B, we next discuss our experimental data. For the nonvanishing central minimum in $I_c(B)$, a critical current asymmetry δ is required and the shift along the magnetic field axis can solely be caused by a finite value of $\bar{\varphi}_M$. Thus there are only two nontrivial parameters (δ_M, δ_B) left to reproduce the remaining features of the experimental data.

If one allows for an asymmetry in the remanent magnetizations only, i.e., $\delta_M \neq 0$ and $\delta_B = 0$, it is not possible to reproduce the experimental $I_c(B)$ at low and high magnetic fields at the same time. The resulting curves can be seen in Fig. 6(a). For large $\delta_M = -3$ [Fig. 6(a) dashed green line], the fit works well for high fields but fails in the first side minima. With a smaller value of $\delta_M = -1.2$ [Fig. 6(a) solid red line], the situation is opposite.

By contrast, the parameter δ_B (with $\delta_M = 0$) leads to a good agreement between the theoretical and experimental $I_c(B)$ pattern. This is shown in Fig. 6(b) where we used $\delta_B = 0.059$. There are only small asymmetries near the side maxima and minima that cannot be reproduced for the case $\delta_M = 0$. If we use both asymmetry parameters, we get an excellent agreement of the theory with the experimental data, as shown in Fig. 6(c) for the $T = 2.65$ K data.

To further test the fit procedure, we now use the $T = 4.2$ K data and assume that the magnetic parameters remain the same as for $T = 2.65$ K. By contrast, δ will change due to a different temperature dependence of j_c^0 and j_c^π, as already discussed above. For $\delta = 0.33$, we get a reasonable agreement, as shown in Fig. 7.

The $T = 4.2$ K fit is apparently not as good as the $T = 2.65$ K fit. However note that, due to the smaller junction resistance, at 4.2 K, the detection limit is much higher and the minima in $I_c(B)$ are limited by the finite-voltage criterion. Still some of the bumps appear at the same values of applied field both in the experimental and theoretical curve.

For the sake of completeness, we also consider the effect of the finite-voltage criterion. Using the expression $V = R\sqrt{I^2 - I_c^2}$ describing the current-voltage characteristics of a Josephson junction in the framework of the resistively shunted junction model,[35,36] we get a corrected $I_c(B)$ via $I_{c,\mathrm{eff}}(B) = \sqrt{(V_{\mathrm{cr}}/R)^2 + I_c(B)^2}$, where $I_c(B)$ refers to the theoretical curve (solid curve in Fig. 7). The corrected curve is shown as dashed (green) line in Fig. 7. As can be seen, the data are reproduced perfectly.

Discussion of the parameters obtained

Finally, we would like to discuss the parameters which are obtained by fitting the experimental data. As already mentioned above, the parameters δ, $\bar{\varphi}_M$, δ_M, and δ_B allow to find the different parameter sets for the two halves of the junction. For the distinction between "0" and "π," additional information is needed, which we get from the reference junctions.

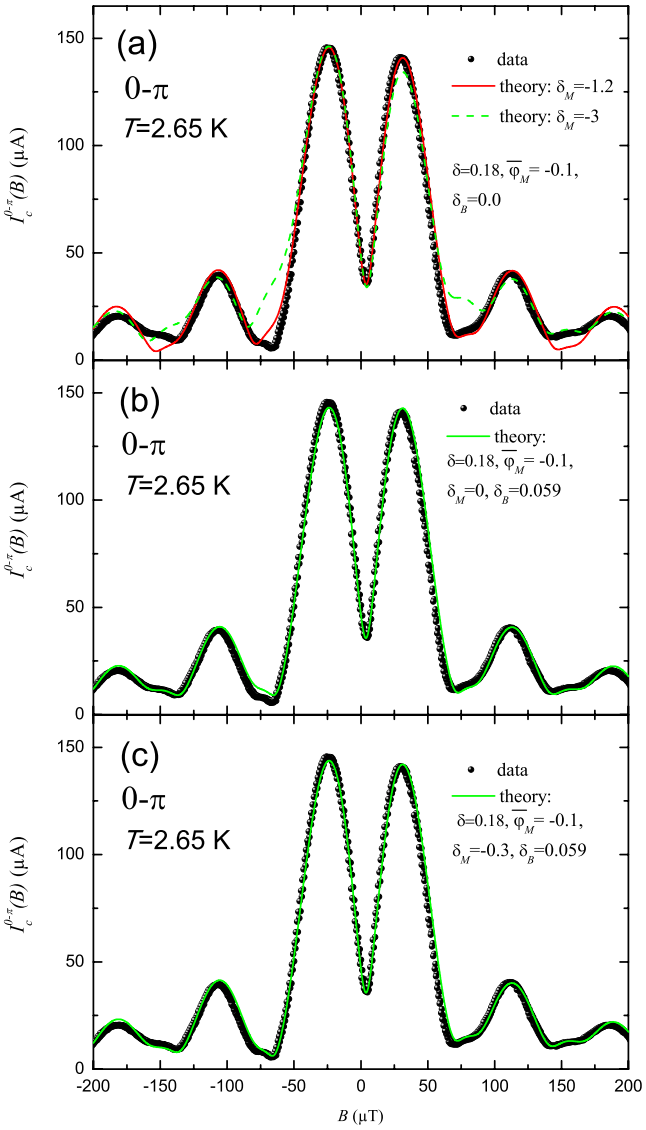

FIG. 6. (Color online) $I_c(B)$ patterns of 0-π junction: comparison of experimental data and fitted magnetic diffraction pattern $I_c^{0\text{-}\pi}(B)$ for $T = 2.65$ K using $\delta = 0.18$ and $\bar{\varphi}_M = -0.1$. In (a) δ_M has been varied at fixed $\delta_B = 0$, in (b) δ_B was varied with fixed $\delta_M = 0$, and in (c) δ_M and δ_B are varied.

The parameter δ allows to extract the absolute values of the critical current densities in the two parts. The obtained values of $j_c^1(T)$ and $j_c^2(T)$ for various temperatures $T = 4.2 \ldots 2.65$ K are shown as open and closed circles in the lower inset of Fig. 4(b) together with the corresponding critical current densities of the reference junctions. We get an almost temperature-independent critical current density j_c^1 in the one half with $j_c^1(4.2\ \mathrm{K}) \approx j_c^1(2.65\ \mathrm{K}) \approx 2.3\ \mathrm{A/cm^2}$. By contrast, for the other part, we find a temperature-dependent current density j_c^2 with $j_c^2(4.2\ \mathrm{K}) \approx 1.2\ \mathrm{A/cm^2}$ to $j_c^2(2.65\ \mathrm{K}) \approx 1.6\ \mathrm{A/cm^2}$. A comparison with the tempera-

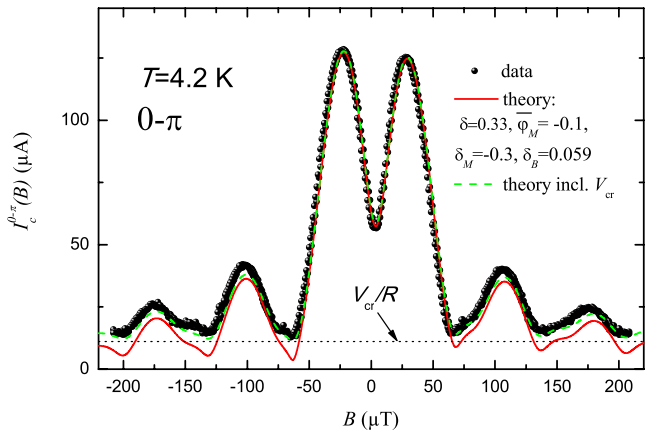

FIG. 7. (Color online) $I_c(B)$ patterns of 0-π junction: comparison of experimental data and fitted magnetic diffraction pattern $I_c^{0-\pi}(B)$ for T=4.2 K (solid line). The dashed line includes the effect of a finite-voltage criterion V_{cr}.

ture dependencies of the reference junctions allows the identification that the first part has to be 0 coupled whereas the second part is π coupled. The absolute values of j_c^0 of the 0 and the 0-π junction are approximately the same whereas j_c^π of the 0-π junction is reduced by ≈ 0.5 A/cm^2 as compared to the π reference junction, although the temperature dependence looks very similar. This indicates a slightly reduced thickness of the F-layer in the π part of the 0-π junction, cf. Fig. 1(b). Taking the data of Ref. 8, the difference in thickness can be estimated to be ≈ 0.7 Å. This may be caused by some gradient of the ferromagnetic thickness along x direction on the chip, as the distance between reference and stepped junctions on the chip is about 2 mm.

The parameters related to a different remanent magnetization in the 0 and the π part, i.e., $\bar{\varphi}_M=-0.1$ and $\delta_M=-0.3$, seem reasonable. The magnetization is on the order of 10^{-3} of a fully saturated magnetization, indicating that the F-layer is in a multidomain state. Note that the resulting magnetization of the π part is larger than the magnetization of the 0 part, which seems realistic due to a thicker F-layer in the π part. In fact, the ratio of the F-layer thicknesses d_2/d_1 is very close to 1, so, assuming that magnetization is proportional to the volume of the F-layer in each part, it is quite difficult to explain the above value of δ_M. However, if one assumes that there is a dead layer of thickness d_{dead}, one can calculate its value from

$$\frac{d_1 - d_{\text{dead}}}{d_2 - d_{\text{dead}}} = \frac{1 + \delta_M}{1 - \delta_M}$$

to be $d_{\text{dead}} \approx 4.7$ nm. This value is somewhat larger than $d_{\text{dead}} \approx 3.1$ nm estimated earlier from a $j_c(d_F)$ fit made for a different run of the same fabrication process.[8] However, as we see from Figs. 6(b) and 6(c), the change in δ_M from 0 to −0.3 affects only the tiny features on the $I_c(B)$ curve. Thus, the value of δ_M cannot be found from this fit very exactly.

Besides the current asymmetry δ, the most important parameter for our experiment is the asymmetry parameter δ_B. Using a finite δ and $\delta_B=0.059$, almost all features could be reproduced very well. The addition of the parameters related to remanent magnetizations lead to minor improvements in the agreement of theory and experiment. In the following, we want to discuss three possible scenarios causing the asymmetry δ_B.

First, the effect could be caused simply via the fabrication procedure of the junction. In the π part of the junction, the SF bilayer was deposited *in situ* whereas the Nb cap layer in the 0 part was deposited after an etching process. Thus the properties, such as the mean-free path and hence the London penetration depth λ, of the Nb cap layers in the two halves could easily differ by few percents.

Second, one could think of a paramagnetic component in the magnetization. As already discussed above, the F-layer is expected to be in a multidomain state with a small net magnetization in-plane. An external field applied in-plane could cause a reconfiguration of the domains. In the two halves, the pinning of the domains may be different due to the different thicknesses and the different treatment. This would result in an asymmetric field-dependent magnetization.

A third possibility is the appearance of an enhanced flux penetration due to inverse proximity effect, causing a correction in the London penetration depth. Due to the reduction of the order parameter in the vicinity of the ferromagnetic layer, the effective penetration depth might be enlarged. In order to estimate this effect, we calculated numerically the space-dependent superfluid density $n_s(z)$ in the superconducting and the ferromagnetic part of the SF bilayer using the quasiclassical approach.[26] Herein we used the parameters of our SF bilayer, which were already obtained in Ref. 26 by fitting the experimental data of Ref. 8. By using the (London) expression $\lambda(z) \propto n_s(z)^{-0.5}$, we obtained the spatial dependence of the penetration depth. Then we used the second London equation $\nabla^2 B(z) = B(z)/\lambda^2(z)$ to calculate the magnetic field $B(z)$ numerically. We define the effective penetration depth as $\lambda_{L,\text{eff}} \equiv \lambda_L \Phi_{\text{eff}}/\Phi$, with Φ_{eff} and Φ being the flux in our SF bilayer with and without inverse proximity corrections. For our SIFS junctions with a thickness $d_F \approx 5$ nm of the ferromagnet and $t_2=400$ nm of the top electrode, we get $\lambda_{L,\text{eff}} = 1.005\lambda_L$ at $T=2.65$ K. Therefore in our case, the inverse proximity corrections are negligible. In addition, the corrections due to inverse proximity effect would be opposite in sign, i.e., $\delta_B < 0$, in contrast to $\delta_B=+0.059$ found for our junction.

By looking at the other two scenarios, it seems natural that the fabrication procedure causes the observed δ_B asymmetry. However at the moment, we cannot exclude a field dependence of the magnetization. A clarification deserves further investigations.

IV. CONCLUSIONS

In this paper, we presented a detailed analysis of the magnetic field dependence of the critical current, $I_c(B)$, in 0, π, and 0-π SIFS Josephson junctions. The length of the junctions is smaller than the Josephson length. The $I_c(B)$ pattern of the 0 and the π junction can be well described by the standard Fraunhofer pattern, valid for a homogenous, short junction. The central maximum of this pattern is typically shifted from zero by some percent of one flux quantum, pointing to a weak in-plane magnetization of the F-layer. The

magnetization is on the order of 10^{-3} of a fully saturated magnetization, indicating that the F-layer is in a multidomain state.

The $I_c(B)$ pattern of the 0-π junction exhibits the central minimum, well known for this type of junction. However, the critical current at this minimum is nonzero, pointing to an asymmetry in the critical current densities in the two halves of the junction. In addition, $I_c(B)$ exhibits asymmetric maxima and bumped minima that cannot be described exclusively by critical current asymmetries. A detailed explanation of these features requires the consideration of asymmetric fluxes generated in 0 and π parts of the junction. A careful analysis of the experimental data and our model showed that the majority of the observed discrepancies are due to a field-dependent asymmetry of the fluxes in the 0 and the π part. The effect could either be caused by a small, field-dependent, in-plane magnetization of the F-layer or by a difference in the penetration lengths, which most naturally can be due to the fabrication technique. In principle, this effect should also be present in the $I_c(B)$'s of the reference junctions. However, here the effect only leads to a small scaling factor for the magnetic field, which is too small to be detectable in experiment, e.g., if the effects of field focusing are considered.

The model discussed in this paper on the basis of 0-π junctions can be extended, e.g., to SIFS junctions having arbitrary steplike $j_c(x)$ profile[37] or laterally ordered ferromagnetic domains.

ACKNOWLEDGMENTS

This work is supported by the Deutsche Forschungsgemeinschaft (DFG) via the SFB/TRR 21 and Projects No. GO 944/3 and KO 1303/3. M. Kemmler acknowledges support by the Carl-Zeiss Stiftung. M. Weides is supported by DFG under Project No. WE 4359/1-1.

*kemmler@pit.physik.uni-tuebingen.de
†Present address: Department of Physics, University of California, Santa Barbara, CA 93106, USA.

[1] L. Bulaevskiĭ, V. Kuziĭ, and A. Sobyanin, JETP Lett. **25**, 290 (1977).
[2] A. I. Buzdin, L. N. Bulaevskiĭ, and S. V. Panyukov, JETP Lett. **35**, 178 (1982).
[3] V. V. Ryazanov, V. A. Oboznov, A. Y. Rusanov, A. V. Veretennikov, A. A. Golubov, and J. Aarts, Phys. Rev. Lett. **86**, 2427 (2001).
[4] H. Sellier, C. Baraduc, F. Lefloch, and R. Calemczuk, Phys. Rev. Lett. **92**, 257005 (2004).
[5] Y. Blum, A. Tsukernik, M. Karpovski, and A. Palevski, Phys. Rev. Lett. **89**, 187004 (2002).
[6] A. Bauer, J. Bentner, M. Aprili, M. L. Della Rocca, M. Reinwald, W. Wegscheider, and C. Strunk, Phys. Rev. Lett. **92**, 217001 (2004).
[7] T. Kontos, M. Aprili, J. Lesueur, F. Genet, B. Stephanidis, and R. Boursier, Phys. Rev. Lett. **89**, 137007 (2002).
[8] M. Weides, M. Kemmler, E. Goldobin, D. Koelle, R. Kleiner, H. Kohlstedt, and A. Buzdin, Appl. Phys. Lett. **89**, 122511 (2006).
[9] A. A. Bannykh, J. Pfeiffer, V. S. Stolyarov, I. E. Batov, V. V. Ryazanov, and M. Weides, Phys. Rev. B **79**, 054501 (2009).
[10] D. Sprungmann, K. Westerholt, H. Zabel, M. Weides, and H. Kohlstedt, J. Phys. D **42**, 075005 (2009).
[11] L. N. Bulaevskiĭ, V. V. Kuziĭ, and A. A. Sobyanin, Solid State Commun. **25**, 1053 (1978).
[12] D. J. Van Harlingen, Rev. Mod. Phys. **67**, 515 (1995).
[13] C. C. Tsuei and J. R. Kirtley, Rev. Mod. Phys. **72**, 969 (2000).
[14] D. A. Wollman, D. J. Van Harlingen, J. Giapintzakis, and D. M. Ginsberg, Phys. Rev. Lett. **74**, 797 (1995).
[15] B. Chesca, R. R. Schulz, B. Goetz, C. W. Schneider, H. Hilgenkamp, and J. Mannhart, Phys. Rev. Lett. **88**, 177003 (2002).
[16] H. J. H. Smilde, Ariando, D. H. A. Blank, G. J. Gerritsma, H. Hilgenkamp, and H. Rogalla, Phys. Rev. Lett. **88**, 057004 (2002).
[17] Ariando, D. Darminto, H. J. H. Smilde, V. Leca, D. H. A. Blank, H. Rogalla, and H. Hilgenkamp, Phys. Rev. Lett. **94**, 167001 (2005).
[18] A. V. Ustinov, Appl. Phys. Lett. **80**, 3153 (2002).
[19] E. Goldobin, A. Sterck, T. Gaber, D. Koelle, and R. Kleiner, Phys. Rev. Lett. **92**, 057005 (2004).
[20] M. L. Della Rocca, M. Aprili, T. Kontos, A. Gomez, and P. Spathis, Phys. Rev. Lett. **94**, 197003 (2005).
[21] S. M. Frolov, D. J. Van Harlingen, V. V. Bolginov, V. A. Oboznov, and V. V. Ryazanov, Phys. Rev. B **74**, 020503(R) (2006).
[22] S. M. Frolov, M. J. A. Stoutimore, T. A. Crane, D. J. Van Harlingen, V. A. Oboznov, V. V. Ryazanov, A. Ruosi, C. Granata, and M. Russo, Nat. Phys. **4**, 32 (2008).
[23] M. Weides, M. Kemmler, H. Kohlstedt, R. Waser, D. Koelle, R. Kleiner, and E. Goldobin, Phys. Rev. Lett. **97**, 247001 (2006).
[24] M. Weides, C. Schindler, and H. Kohlstedt, J. Appl. Phys. **101**, 063902 (2007).
[25] J. Pfeiffer, M. Kemmler, D. Koelle, R. Kleiner, E. Goldobin, M. Weides, A. K. Feofanov, J. Lisenfeld, and A. V. Ustinov, Phys. Rev. B **77**, 214506 (2008).
[26] A. S. Vasenko, A. A. Golubov, M. Y. Kupriyanov, and M. Weides, Phys. Rev. B **77**, 134507 (2008).
[27] A. F. Volkov and K. B. Efetov, Phys. Rev. Lett. **103**, 037003 (2009).
[28] M. Weides, H. Kohlstedt, R. Waser, M. Kemmler, J. Pfeiffer, D. Koelle, R. Kleiner, and E. Goldobin, Appl. Phys. A **89**, 613 (2007).
[29] V. A. Oboznov, V. V. Bol'ginov, A. K. Feofanov, V. V. Ryazanov, and A. I. Buzdin, Phys. Rev. Lett. **96**, 197003 (2006).
[30] R. Monaco, G. Costabile, and N. Martucciello, J. Appl. Phys. **77**, 2073 (1995).
[31] S. A. Ahern, M. J. C. Martin, and W. Sucksmith, Proc. R. Soc. London **248**, 145 (1958).
[32] M. Weides, Appl. Phys. Lett. **93**, 052502 (2008).
[33] I. Veshchunov, V. Oboznov, A. Rossolenko, A. Prokofiev, L. Vinnikov, A. Rusanov, and D. Matveev, JETP Lett. **88**, 758 (2008).
[34] J. H. Xu, J. H. Miller, and C. S. Ting, Phys. Rev. B **51**, 11958 (1995).
[35] W. C. Stewart, Appl. Phys. Lett. **12**, 277 (1968).
[36] D. McCumber, J. Appl. Phys. **39**, 3113 (1968).
[37] M. Weides, IEEE Trans. Appl. Supercond. **19**, 689 (2009).